Historical Information Aware Unequal Error Protection of Scalable HEVC/H.265 Streaming Over Free Space Optical Channels

YONGKAI HUO[1], CHENG ZHOU[2], JUNYI JIANG[1], AND LAJOS HANZO[1], (Fellow, IEEE)

[1]School of Electronics and Computer Science, University of Southampton, Southampton, SO17 1BJ, U.K.
[2]Hubei Key Laboratory of Intelligent Wireless Communications, South-Central University for Nationalities, Wuhan 430071, China

Corresponding author: L. Hanzo (lh@ecs.soton.ac.uk)

ABSTRACT Free space optical (FSO) systems are capable of supporting high data rates between fixed points in the context of flawless video communications. Layered video coding facilitates the creation of different-resolution subset layers for variable-throughput transmission scenarios. In this paper, we propose historical information aware unequal error protection (HA-UEP) for the scalable high efficiency video codec used for streaming over FSO channels. In particular, the objective function (OF) of the current video frame is designed based on historical information of its dependent frames. By optimizing this OF, specific subset layers may be selected in conjunction with carefully selected forward error correction coding rates, where the expected video distortion is minimized and the required bitrate is reduced under the constraint of a specific throughput. Our simulation results show that the proposed system outperforms the traditional equal error protection (EEP) scheme by about 4.5 dB of E_b/N_0 at a peak signal-to-noise ratio of 33 dB. From a throughput-oriented perspective, HA-UEP is capable of reducing the throughput to about 30% compared with that of the EEP benchmarker, while achieving an E_b/N_0 gain of 4.5 dB.

INDEX TERMS HEVC, video streaming, free optical channels, unequal error protection, scalable video.

I. INTRODUCTION

In recent years, low-delay lip-synchronized wireless video communications became a reality and the road to this era is detailed in [1]. In 2015, Cisco reported the mobile data traffic forecast seen in Fig. 1, which shows that the video data traffic is predicted to grow from 55% to 72% of the total tele-traffic in during the years 2014 to 2019. On the other hand, high-bandwidth optical wireless communications may be necessitated for meeting the challenge of flawless video communications.

The structure of this treatise is shown in Fig. 2. Specifically, the background of layered video communications for transmission over free-space optical channels will be introduced in Section I. Section II details the architecture of our proposed system. The coding-rate optimization of the system is detailed in Section III. The performance of our optimized scheme using a recursive systematic convolutional (RSC) codec is characterized in Section IV using multiple scalable video sequences of different motion characteristics. Finally, we offer our conclusions in Section V. In the rest of this section, we introduce the background of layered video communications for transmission over free-space optical channels.

A. SCALABLE EXTENSION OF HEVC/H.265

Layered video compression [3]–[6] encodes a video sequence into multiple layers, as illustrated by Fig. 3, which enables us to progressively refine the reconstructed video quality at the receiver. A layered video scheme is displayed in Fig. 3, where the video sequence captured from the scene is encoded into four layers by the layered video encoder, namely $l_1 \sim l_4$, where layer l_i ($2 \leq i \leq 4$) depends on layer l_{i-1} for decoding, while layer l_i improves the video quality of layer l_{i-1}. Generally, the most important layer, namely l_1 is referred to as the base layer (BL) and the less important layers $l_2 \sim l_4$ are termed as enhancement layers (ELs), which rely on the BL. Furthermore, an EL may be further relied upon by less important ELs. Again, when the BL or an EL is lost or corrupted during its transmission, the dependent layers cannot be utilized by the decoder and must be dropped.

A number of layered video coding techniques have been investigated and/or standardized [7], such as the partitioned
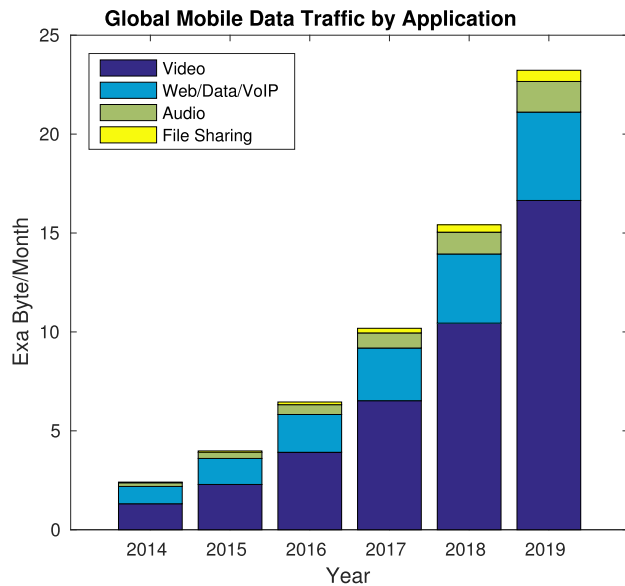
Global Mobile Data Traffic by Application

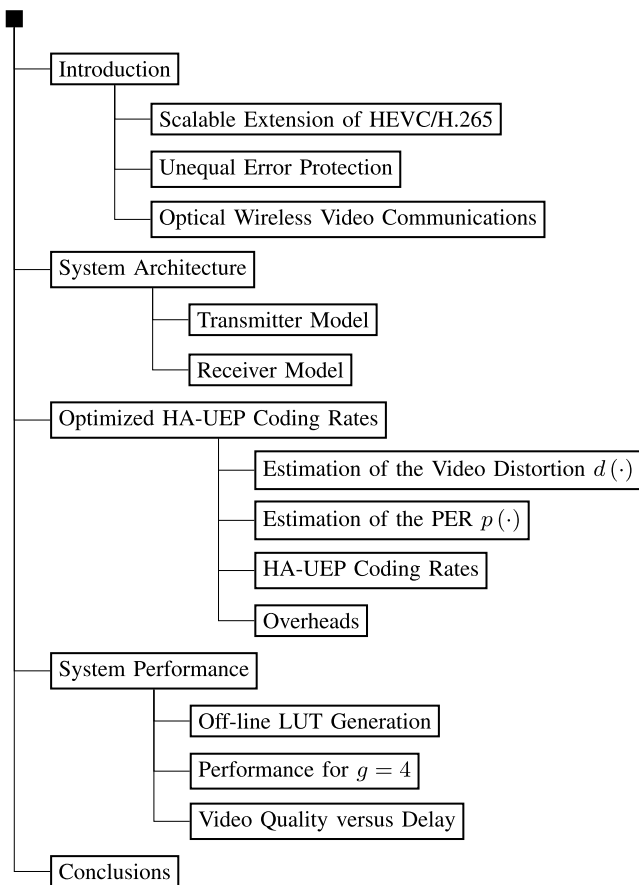**FIGURE 1.** Mobile data traffic report by Cisco.

FIGURE 2. The structure of the paper.

mode video coding of [5], the multiview profile (MVP) of [3] developed by the moving picture expert group (MPEG), the scalable video coding (SVC) [4], [5] extension of H.264/AVC [5] and the SVC profile of the H.265 high

efficiency video coding (HEVC) arrangement [8], [9]. More-over, scalable coding techniques are also widely employed in the standard profile of HEVC. Here we focus our attention on the scalable extension of HEVC, while a range of other standards were introduced in [7].

In the scalable extension of HEVC, the main types of scal-ability are temporal-, spatial-, and quality-based scalability. Spatial scalability and temporal scalability describe cases in which a sub-bitstream represents the source content at a reduced spatial resolution and frame rate, respectively. In case of quality-scalability, which is also referred to as signal-to-noise ratio (SNR) scalability or fidelity-scalability, the sub-bitstream provides a reduced reconstructed video quality.

Fig. 4 depicts the simplified block diagram of scalable HEVC (SHVC) for spatial- and quality-scalable coding for two layers. For spatial-scalability, the input video is down-sampled and fed into the base layer encoder of Fig. 4, while the original video is directly input to the enhancement layer encoder of Fig. 4. For quality-scalability, the ``Downsam-pler'' block of Fig. 4 is ignored. The outputs of both encoders are multiplexed in order to form the final scalable bitstream containing multiple layers.

B. UNEQUAL ERROR PROTECTION

It is intuitive to differently protect the BL an ELs for the sake of improved error-resilience. Explicitly, unequal error protection (UEP) was firstly proposed by Masnick and Wolf in [11], which allocates stronger FEC to the more important data, while dedicating weaker FEC to the less important video parameters. Four categories of UEP techniques were reviewed in [7], namely transceivers based on UEP schemes [26], packet-level FEC Schemes [27], bit-level FEC Schemes [22], [24] and cross-layer operation aided schemes [28]. Here we concentrate our attention on the family of bit-level FEC schemes with the major contributions listed in Table 1, while the review of other schemes is detailed in [7].

The authors of [12] minimized the mean video distortion by non-uniformly distributing the redundancy imposed by the turbo code between the successive video frames, where the H.263 video codec was employed. Low-density parity-check (LDPC) code based UEP was investigated in [17]. The UEP performance of data-partitioned [5] H.264/AVC video streaming systems using RSC codes was evaluated in [21], while turbo coded modulation [29] based UEP was investigated in [18], where both the cutoff rates and the channel capacity of each of the UEP levels was determined. The authors of [19] considered the unequal importance of both the video-frames in a GOP and the significance of the diverse MBs in a video frame for transmission over wireless channels, where a prompt and efficient bit-rate allocation scheme was also investigated. However, only three protection classes were discussed in [19], which limits the attainable system performance. The authors of [23] demon-strated that the side information (SI) values within different positions of the Wyner-Ziv (WZ) frames have different error probability. Hence UEP of these non-uniformly distributed
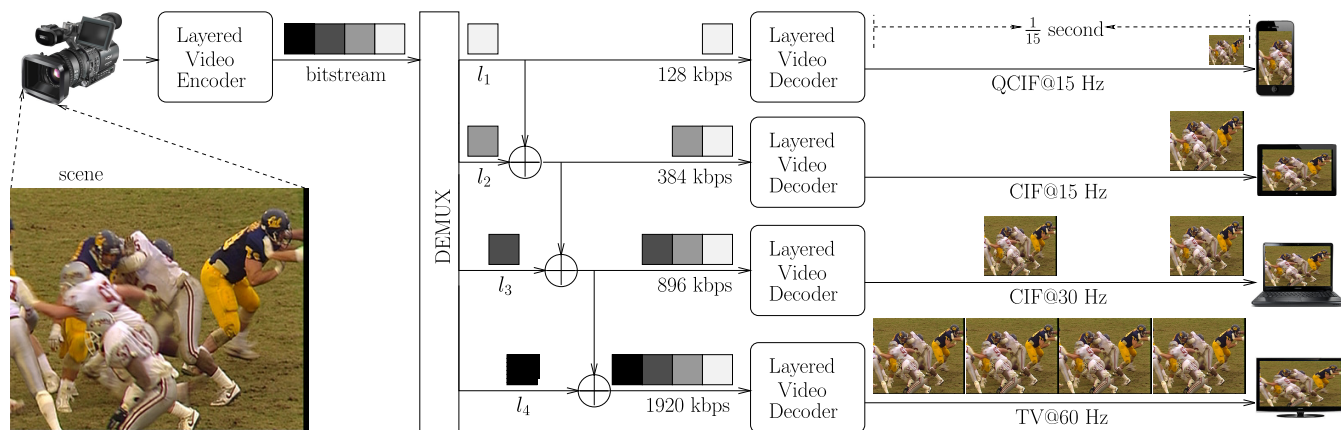
FIGURE 3. Architecture of a layered video scheme [2], where the video quality is refined gradually. Common intermediate format (CIF) and quarter CIF (QCIF) indicate resolutions of (352×288) and (176×144), respectively.
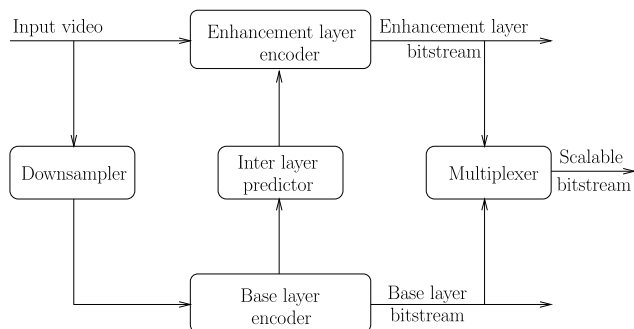

FIGURE 4. Simplified block diagram of a scalable encoder with two layers [10].

SI values was employed for the sake of reducing the required bitrate in the context of distributed video coding (DVC) [30], [31]. The authors of [2] and [7] developed bit-level inter-layer coded FEC (IL-FEC) arrangements for layered video telephony over wireless fading channels in [22] relying on soft-decoded RSC, as well as turbo and self-concatenated convolutional codes, respectively, where the systematic bits of the BL are implanted into the ELs at the transmitter. At the receiver, the BL's bits implanted into the ELs may be beneficially exploited for correcting the BL. The above-mentioned IL-FEC technique of [22] was also combined with the UEP philosophy for the sake of further improving the attainable system performance. In [24], the authors proposed a technique for finding the optimized coding rates for coded bit-streams "on-the-fly" at the transmitter, which optimized the IL-FEC coded system performance. Three-Dimensional (3D) stereoscopic video relying on depth-map format was investigated in [25] for transmission over noisy channels, where suitable color and depth quantization parameters as well as the FEC coding rates were used for UEP.

C. OPTICAL WIRELESS VIDEO COMMUNICATIONS

Optical wireless communication (OWC) transmits information using optical carries through unguided propagation media. Furthermore, outdoor terrestrial OWC links operate close to the infrared (IR) band, which are referred to as free space optical (FSO) links. FSO systems [32] support high-rate communication between two fixed points over distances up to several kilometers, which have a high optical bandwidth available, hence potentially competing with fiber optic links [32], [33]. FSO systems have attracted substantial research attention as a potential wireless link between the end user and the existing fiber optic infrastructure, which are capable of supporting ultra high definition video communications.

Yet, there is a paucity of contributions focused on video communications of video over optical wireless channels. In [34], an LDPC code was employed for real-time video transmission over turbulent temporally correlated optical wireless channels. Different optical transmission media and different orthogonal frequency division multiplexing (OFDM) transmission frequency bands were evaluated experimentally in [35]. Furthermore, the suitability of using optical-wireless networks for high definition (HD) video broadcasting [35] has been evaluated.

Against this background, in this treatise, we consider the scenario of transmitting SHVC over FSO channels, where a space–time block code (STBC) is employed for the sake of attaining diversity gain. We are motivated by the fact that any enhancement layer of the current video frame becomes useless without the successfully received more important layers, including the dependent layers of the current video frame and the historical video frames. Hence, for each frame, we propose Historical information Aware Unequal Error Protection (HA-UEP) for transmitting SHVC over FSO channels. Specifically, given a particular throughput upper-bound, for each frame, our objective function (OF) is designed based on the layer-dependencies of both the intra-frame and inter-frame video, namely based on the current frame and historical frames. By optimizing this OF, a specific subset of the layers may be selected together with the most appropriate forward error correction (FEC) coding rates, where the expected video

TABLE 1. Major contributions on unequal error protection for video communications.

Year	Author(s)	Contribution
1967	Masnick and Wolf [11]	first proposed UEP, which allocates stronger FEC to the more important data.
2004	Marx and Farah [12]	minimized the mean distortion by non-uniformly distributing redundancy among the successive video frames.
2006	Pavlushkov *et al.* [13]	studied the UEP capabilities of convolutional code (CC), while rate-compatible convolutional codes (RCPC) was proposed by Hagenauer [14].
	Kumar and Milenkovic [15]	proposed a new family of UEP codes, based on LDPC [16] component codes, where the order of decoding and the choice of the component codes jointly determine the level of error protection.
2007	Rahnavard *et al.* [17]	conceived an UEP scheme using partially regular LDPC codes.
2008	Aydinlik and Salehi [18]	investigated UEP based turbo coded modulation, where both the channel capacity and the cutoff rates of the UEP levels were determined.
	Chang *et al.* [19]	considered the unequal importance of the frames in a group of pictures (GOP), as well as that of the macroblocks in a video frame.
2009	Chang *et al.* [20]	considered the different importance of the I-frame and of the P-frames within a GOP.
2011	Nasruminallah and Hanzo [21]	evaluated the UEP performance of data-partitioned H.264/AVC video streaming systems using RSC codes.
2013	Huo *et al.* [22]	developed a bit-level inter-layer coded FEC (IL-FEC) scheme for layered wireless video steaming relying on a soft-decoded FEC code, where the systematic bits of the BL are implanted into the ELs at the transmitter.
	Micallef *et al.* [23]	conceived UEP for side information (SI) values at different positions of the Wyner-Ziv (WZ) frames for the sake of reducing the bitrate in distributed video coding (DVC).
2014	Huo *et al.* [24]	proposed a technique for finding the optimized coding rates for coded bitstreams "on-the-fly" at the transmitter, which optimizes the IL-FEC coded system performance.
2015	Vosoughi *et al.* [25]	studied UEP for the stereoscopic video represented in the depth-map format.

distortion is minimized under the constraint of a limited throughput. The rationale and novelty of this paper is summarized as follows.

1) *We set out to optimize soft-decoding bit-level unequal error protected scalable HEVC communication over FSO channels.*
2) *The OF of optimization is designed by considering both the current frame and historical frames.*
3) *We design the OF for the sake of finding the most appropriate subset of layers together with the best code rates under the constraint of a limited throughput.*
4) *HA-UEP is capable of reducing the bitrate to 30% compared to that of the EEP benchmarker, while achieving an E_b/N_0 gain of 4.5 dB.*

II. SYSTEM ARCHITECTURE

In this section, we introduce our proposed HA-UEP scheme conceived for SHVC-aided communications over FSO channels, as seen in Fig. 5. We focus our attention on the general architecture of the transmitter and receiver, while the "Code Rate Optimization" block of Fig. 5 will be detailed in Section III. Let us commence by defining the notations of Fig. 5 in Table 2.

A. TRANSMITTER MODEL

At the transmitter of Fig. 5, the video source signal U is compressed using the SHVC encoder, generating the SHVC bitstream, which is then de-multiplexed into the bitstreams of layers $l_{i,1}, \ldots, l_{i,n}$ by the *DEMUX* block of Fig. 5. Meanwhile,
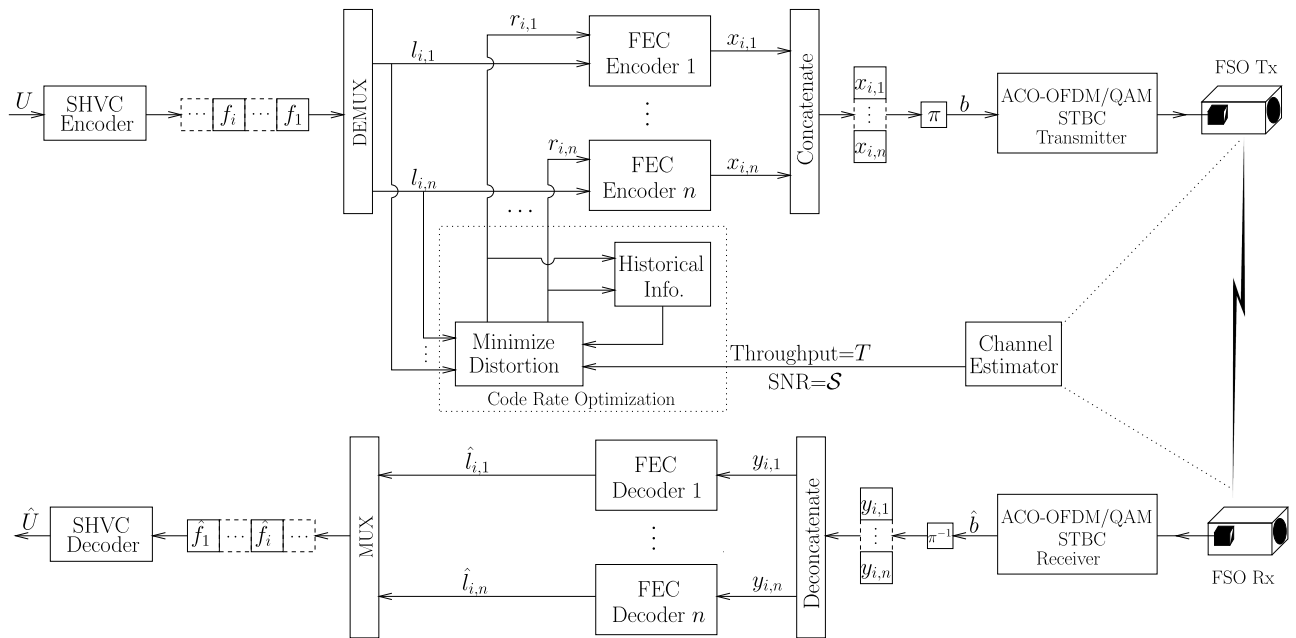
FIGURE 5. Block diagram of the proposed HA-UEP aided SHVC communications over FSO channels , where *n* is the number of layers and $r_{i,1}, \cdots, r_{i,n}$ represent the code rates of the FEC encoders $1, \cdots, n$ for frame *i*, respectively. The "Code Rate Optimization" block will be detailed in Section III.

TABLE 2. Symbol definition, where $i \geq 1$, $1 \leq j \leq n$ indicate the frame index and layer index, respectively.

Symbol	Definition
n	number of layers considered in the system
$\mathcal{S}$	the estimated SNR for transmission of the video
f_i	bitstream of frame i
$l_{i,,j}$	layer j of frame i
$x_{i,j}$	FEC encoded version of layer $l_{i,j}$
$r_{i,j}$	FEC coding rate of layer $l_{i,j}$
T	the maximum allowed throughput expressed in bits per second (BPS) of the transceivers
$y_{i,j}$	the received version of sequence $x_{i,j}$
$\hat{l}_{i,j}$	the decoded version of layer $l_{i,j}$
$\hat{f}_i$	the decoded bitstream of frame i

the information of layers $l_{i,1}, \ldots, l_{i,n}$ is input to the "Code Rate Optimization" block of Fig. 5, which will generate the optimized coding rates $r_{i,1}, \cdots, r_{i,n}$ for the layers $l_{i,1}, \ldots, l_{i,n}$, respectively. Afterwards, the resultant n layers are encoded as follows:

1) The n bit sequences $l_{i,1}, \ldots, l_{i,n}$ will be encoded by the FEC encoders $1, \ldots, n$ of Fig. 5, where the coding rates $r_{i,1}, \cdots, r_{i,n}$ are generated by the "Code Rate

Optimization" block, respectively. This results in the encoded bit sequences $x_{i,1}, \ldots, x_{i,n}$, respectively.

2) The bit sequences $x_{i,1}, \ldots, x_{i,n}$ are then concatenated into a joint bitstream for transmission. The interleaver π of Fig. 5 is employed for interleaving the joint bitstream.

3) The interleaved joint bit sequence is encoded by the STBC. Specifically, this joint bit sequence, denoted as b is firstly mapped to the $|b|/M$-length quadrature amplitude modulation (QAM) symbol vector, which is then mapped onto the M substreams of the STBC-aided asymmetrically clipped optical (ACO)-OFDM [36] transmitter designed in [37] and then transmitted by the M FSO apertures of Fig. 5.

4) The M symbol sub-streams are then transmitted over the $(N \times M)$-element multiple-input and multiple-output (MIMO) FSO turbulence channel obeying the Gamma-Gamma distribution [38].

Finally, the STBC scheme's output sequence is transmitted over free space optical channels.

B. RECEIVER MODEL

The free space optical receiver of Fig. 5 is employed for detecting the optical signals followed by processing the SHVC video bitstream as follows:

1) After optical to electronic conversion, the N received signal substreams are passed through the ACO-OFDM/ QAM demodulator to extract the complex-valued sequences of Fig. 5. Assuming perfect knowledge of the channel at the receiver, the joint Maximum-Likelihood (ML) detection of the received signal can

be carried out. Finally, the estimate of the transmitted bit-block $\hat{b}$ can be obtained by QAM-demodulating. More details of the FSO system may be found in [37].

2) After the STBC decoding process, the detected signals will then be deinterleaved by the deinterleavers π^{-1} of Fig. 5, generating the soft version of the sequences $x_{i,1}, \ldots, x_{i,n}$, namely $y_{i,1}, \ldots, y_{i,n}$.

3) The soft information $y_{i,j}$ is decoded by the FEC decoder j of Fig. 5, which generates the bit sequence $\hat{l}_{i,j}$, representing the estimated version of layer $l_{i,j}$.

Finally, the estimated layers $\hat{l}_{i,1}, \cdots, \hat{l}_{i,n}$ are then assembled into a SHVC bitsteam by the "MUX" block of Fig. 5, which will be invoked for reconstructing the video $\hat{U}$.

III. OPTIMIZED HA-UEP CODING RATES

In SHVC, intra-coded frames (I), predicted frames (P) and bi-directional predicated frames (B) may be generated, which are exemplified by the IBPBP frame-structure displayed in Fig. 6a. In this section, we focus our attention on the low-delay profile of the SHVC scheme for the sake of supporting lip-synchronization, where the B frames are disabled. Nonetheless, the proposed techniques may be readily extended to B frames. The layer dependency of the IPPP coding structure is displayed in Fig. 6b, where solid arrows and dashed arrows represent the intra-frame and inter-frame dependency, respectively. Moreover, the I frames or random access points (RAC)[1] of clean decoder refresh (CDR) or instantaneous decoding refresh (IDR) pictures are inserted every m frames. Note that the dependency $l_{i,j} \rightarrow l_{i,j+1}$ implies that $l_{i,j+1}$ depends on $l_{i,j}$, which indicates that layer $l_{i,j+1}$ will become useless, when $l_{i,j}$ is corrupted.

Below, we detail the "Code Rate Optimization" block of Fig. 5, which aims for finding the specific FEC coding rates $r_{i,1}, \cdots, r_{i,n}$ of encoding the different-significance layers $l_{i,1}, \cdots, l_{i,n}$ of frame f_i for the sake of minimizing the expected distortion of the reconstructed video at the receiver. Furthermore, we consider the time slot of g frames as an optimization group limited by the throughput upper bound of $T \cdot \frac{g}{\mathfrak{F}}$, where $\mathfrak{F}$ is the FPS scanning-rate of the considered video. More specifically, we chose the first group of g frames for the sake of simplicity.[2] For example, we denote the number of bits in the first group of g frames as $|f_1|, \cdots, |f_g|$. For a specific frame of size f_i, $1 \leq i \leq g$, we simply allocate the corresponding throughput as[3]

$$t_i = T \cdot \frac{g}{\mathfrak{F}} \cdot \frac{|f_i|}{\sum\limits_{j=1}^{g} |f_j|}, \tag{1}$$

---

[1] RAC break the dependency among frames, which refresh the decoding reference frames for the sake of accessing frames of a video stream randomly. They also improve the robustness of a video stream by reducing the coding efficiency.

[2] We assume that there are one I frame and $(g-1)$ P frames in the optimization group for the sake of simplicity.

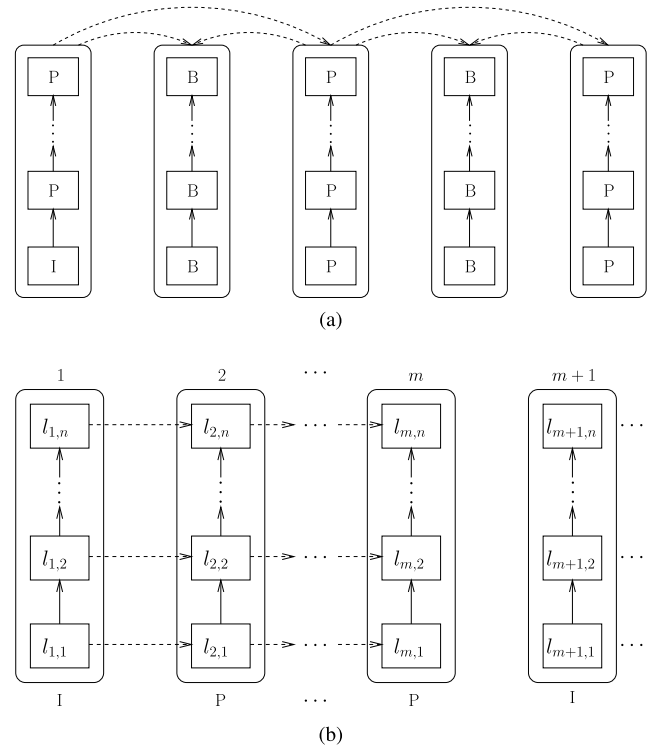[3] This linear throughput allocation strategy will be improved in our future study.

(a)

(b)

FIGURE 6. Frame and layer dependency of SHVC, where solid arrow → and dashed arrow ⇢ indicate intra-frame and inter-frame dependency, respectively. (a) Frame dependency of IBPBP structure with decoding order of IPBPB. (b) Layer dependency of IPPP structure with intra-period of m.

which is the upper bound of the encoded version of n layers, hence we have $\sum\limits_{j=1}^{n} |x_{i,j}| \leq t_i$. In the following, we minimize the distortion of transmitting the layers $l_{i,1}, \ldots, l_{i,n}$ by deriving the specific FEC coding rates $r_{i,1}, \ldots, r_{i,n}$. Moreover, for simplicity we assume that the dependency of the layers is characterized by $l_{i,j} \rightarrow l_{i,j+1}$, namely $l_{i,j+1}$ depends on $l_{i,j}$, $1 \leq j \leq n$. In this section, we illustrate our algorithm by focusing on frame f_i, $1 \leq i \leq g$. Based on the notations of Section II, we commence by defining the mathematical notations in Table 3.

We characterize the video distortion, in terms of peak signal-to-noise ratio (PSNR) degradation, caused by the n erroneous layers as $\mathfrak{D}\left(\mathcal{S}, l_{i,1}, \cdots, l_{i,n}, r_{i,1}, \cdots, r_{i,n}\right)$, when the coding rates of $r_{i,1}, \cdots, r_{i,n}$ and SNR=$\mathcal{S}$ are employed. In this paper, our objective is to derive the specific code rates $r_{i,1}, \cdots, r_{i,n}$, which minimize the expected PSNR degradation $\mathfrak{D}\left(\mathcal{S}, l_{i,1}, \cdots, l_{i,n}, r_{i,1}, \cdots, r_{i,n}\right)$. Furthermore, the distortion caused by the corruption of $l_{i,j}$ may be calculated as $d\left(l_{i,j}\right) \cdot p\left[\psi(l_{i,j})\right] \cdot p\left(s_i, |l_{i,j}|, r_{i,j}\right)$. The expected distortion $\mathfrak{D}\left(\mathcal{S}, l_{i,1}, \cdots, l_{i,n}, r_{i,1}, \cdots, r_{i,n}\right)$ may be evaluated as

$$\mathfrak{D}\left(\mathcal{S}, l_{i,1}, \cdots, l_{i,n}, r_{i,1}, \cdots, r_{i,n}\right)$$
$$= \sum_{j=1}^{n} d\left(l_{i,j}\right) \cdot p\left(s_i, |l_{i,j}|, r_{i,j}\right) \cdot p\left[\psi(l_{i,j})\right]. \tag{2}$$

Symbol	Definition
t_i	the allocated throughput for frame i
$\mathfrak{F}$	FPS of the video
N_0	variance of Gaussian noise
r_i	overall coding rate of frame f_i
s_i	estimated transmit SNR for transmitted bit for frame f_i
E_b	normalized overall transmit power for each information bit of layers $l_{i,1}, \cdots, l_{i,n}$
e_i	estimated transmit power for each FEC encoded bit of $x_{i,1}, \cdots, x_{i,n}$ of frame f_i
$|l_{i,j}|$	bit length of layer j in frame i
$|x_{i,j}|$	bit length of FEC encoded layer i
$d(l_{i,j})$	video distortion caused by the corruption of layer $l_{i,j}$
$\psi(l_{i,j})$	the set of dependent layers of layer $l_{i,j}$
$p[\psi(l_{i,j})]$	the probability that the layer set $\psi(l_{i,j})$ is correctly decoded
$p(s, l, r)$	the expected packet error probability at the receiver, where l is the packet length input to the FEC encoder with rate r and transmitted at SNR s

Hence, our objective function (OF) invoked may be formulated as

$$\underset{r_{i,1}, \cdots, r_{i,n}}{\arg \min} \mathfrak{D}\left(\mathcal{S}, l_{i,1}, \cdots, l_{i,n}, r_{i,1}, \cdots, r_{i,n}\right)$$

$$= \underset{r_{i,1}, \cdots, r_{i,n}}{\arg \min} \sum_{j=1}^{n} d\left(l_{i,j}\right) \cdot p\left(s_i, |l_{i,j}|, r_{i,j}\right) \cdot p\left[\psi(l_{i,j})\right],$$

$$(3)$$

subject to the conditions of

$$\begin{cases} \sum_{j=1}^{n} |x_{i,j}| \leq t_i \\ \sum_{j=1}^{n} |x_{i,j}| \cdot e_i = \sum_{j=1}^{n} |l_{i,j}| \cdot E_b, \end{cases} \quad (4)$$

where Eq. (4) limits the bitrate available for transmitting the n encoded layers and ensures that an equal amount of power is assigned to $r_{i,1}, \cdots, r_{i,n}$.

In Sections III-A and III-B, we derive the components of Eq. (3), namely the video distortion $d\left(l_{i,j}\right)$ and the conditional packet error ratio (PER) $p\left(s_i, |l_{i,j}|, r_{i,j}\right)$, respectively. Afterwards, we derive the solution of the OF in Eq. (3) for determining the optimized coding rates in Section III-C.

Finally, Section III-D discusses the transmission overheads imposed by the proposed techniques.

A. ESTIMATION OF THE VIDEO DISTORTION d (·)

The video distortion $d\left(l_{i,j}\right)$ is estimated in a similar manner to the procedure of [7], [24], and [39], where the distortion $d\left(l_{i,j}\right)$, $1 \leq j \leq n$ may be obtained by decoding the bitstream in the presence of a corrupted layer $l_{i,j}$. Alternatively, the solutions of [19], [40], and [41] may be applied in our system.
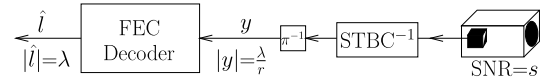

FIGURE 7. The FSO reception, STBC decoding and FEC decoding process at the receiver.

B. ESTIMATION OF THE PER p (·)

Fig. 7 describes the receiver shown in Fig. 5, where the soft information sequence of length $|y| = \frac{\lambda}{r}$ is input to the FEC decoder generating the estimated bits $\hat{l}$ of length $\left|\hat{l}\right| = \lambda$. Moreover, r is the coding rate of the FEC codec and the signals are received at SNR s. Based on the constant value l, the PER of $\hat{l}$ in Fig. 7 depends on the parameters s and r, which may be expressed as $p(s, l, r)$.

The burst error distribution of non-iterative codecs has been investigated in [24] and [42], which is independent of the packet length. Let us now consider a non-iterative decoded packet having a length of $(n_1 \times n_2)$ bits. Then this packet may be partitioned either into n_1 packets, each carrying n_2 bits or n_2 packets associated with n_1 bits each. Assuming that $p(n_i)$ indicates the PER of the n_i-bit packet, the PER $p(n_1 \cdot n_2)$ may be estimated as

$$p(n_1 \cdot n_2) = 1 - [1 - p(n_2)]^{n_1}, \quad (5)$$

where $p(n_2)$ is the PER of the n_1-bit packets. Similarly, we have $p(n_1 \cdot n_2) = 1 - [1 - p(n_1)]^{n_2}$. Then, for arbitrary numerical values of n_1, n_2 we have

$$p(n_1) = 1 - [1 - p(n_2)]^{\frac{n_1}{n_2}}. \quad (6)$$

Upon assuming that n_1, n_2 of Eq. (6) are given by $|l_{i,j}|$ and l, respectively, the PER $p(s_i, |l_{i,j}|, r_{i,j})$ in the OF of Eq. (3) may be estimated as

$$p\left(s_i, |l_{i,j}|, r_{i,j}\right) = 1 - \left[1 - p\left(s_i, l, r_{i,j}\right)\right]^{\frac{|l_{i,j}|}{\lambda}}, \quad (7)$$

where l is the packet length input to the FEC encoder of Fig. 7. More information about this estimation process is provided in [7] and [24].

Below, we firstly solve the function $p(s, l, r)$ by simulating the decoding process of Fig. 7 based on the variables s, r and the constant value l, which generates the look-up table (LUT) $\hbar(s, r)$, characterized by the "simulated" surface seen in Fig. 8. Then we may solve $p(s, l, r)$ by searching
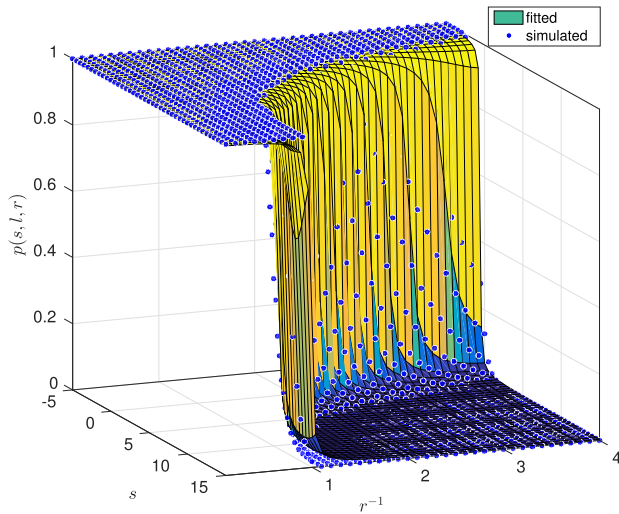
FIGURE 8. Simulated surface of $\hbar(s, r)$ versus fitted using the model of $\frac{1}{\pi} \arctan(a_2 s^2 + a_1 s + b_2 r^{-2} + b_1 r^{-1} + c_0) + \frac{1}{2}$, where $\lambda = 1000$ is employed.

the LUT $\hbar(s, r)$. Alternatively, as indicated by the ''fitted'' surface of Fig. 8, we modeled the the LUT $\hbar(s, r)$ using the mathematical model

$$\hbar(s, r) = \frac{1}{\pi} \arctan(a_2 s^2 + a_1 s + b_2 r^{-2} + b_1 r^{-1} + c_0) + \frac{1}{2}, \tag{8}$$

where we have $a_1 = -14.02$, $a_2 = 0.5219$, $b_1 = -85.24$, $b_2 = 10.37$, $c_0 = 166.9$. Based on the definition of $\hbar(s, r)$, the function $p(s, l, r)$ may be simplified to

$$p(s, l, r) = \hbar(s, r). \tag{9}$$

Then the PER estimation of Eq. (7) may be solved based on the function $\hbar(s, r)$ as

$$p\left(s_i, \left|l_{i,j}\right|, r_{i,j}\right) = 1 - \left[1 - \hbar\left(s_i, r_{i,j}\right)\right]^{\frac{|l_{i,j}|}{\lambda}}. \tag{10}$$

Finally, by substituting Eq. (10) into Eq. (3), the expected video distortion $\mathfrak{D}\left(S, l_{i,1}, \cdots, l_{i,n}, r_{i,1}, \cdots, r_{i,n}\right)$ may be further formulated using $\hbar(s, r)$ as

$$\mathfrak{D}\left(S, l_{i,1}, \cdots, l_{i,n}, r_{i,1}, \cdots, r_{i,n}\right)$$
$$= \sum_{j=1}^{n} d\left(l_{i,j}\right) \cdot \left[1 - \left[1 - \hbar\left(s_i, r_{i,j}\right)\right]^{\frac{|l_{i,j}|}{\lambda}}\right] \cdot p\left[\psi(l_{i,j})\right], \tag{11}$$

C. HA-UEP CODING RATES

We note from Fig. 6b that layer $l_{i,j}$ of frame j depends on layer $l_{i-1,j}$. Hence layer $l_{i,j}$ depends on all the layers within the

set $\psi(l_{i-1,j})$, which is the dependent layers of layer $l_{i-1,j}$. Furthermore, layer $l_{i,j}$ also depends on the layer $l_{i,k}$ of frame k, $1 \le k < j$. Then, the dependent set $\psi(l_{i,j})$ of the layer $l_{i,j}$ may be expressed as

$$\psi(l_{i,j}) = \begin{cases} \bigcup\limits_{k=1}^{j-1} l_{i,k} \bigcup \psi(l_{i-1,j}), & i > 0 \\ \varnothing, & i \le 0. \end{cases} \tag{12}$$

Based on Eq. (10), we may derive the probability $p\left(l_{i,j}\right)$ that layer $l_{i,j}$ is successfully recovered as

$$p\left(l_{i,j}\right) = 1 - p\left(s_i, \left|l_{i,j}\right|, r_{i,j}\right)$$
$$= \left[1 - \hbar\left(s_i, r_{i,j}\right)\right]^{\frac{|l_{i,j}|}{\lambda}}. \tag{13}$$

Correspondingly, for arbitrary $1 \le j \le n$, the probability $p\left[\psi(l_{i,j})\right]$ that the dependent set $\psi(l_{i,j})$ in Eq. (12) is successfully recovered, may be recursively calculated as

$$p\left[\psi(l_{i,j})\right]$$
$$= \begin{cases} p\left[\psi(l_{i-1,j})\right] \cdot \prod\limits_{k=1}^{j-1} \left[1 - \hbar\left(s_i, r_{i,j}\right)\right]^{\frac{|l_{i,j}|}{\lambda}}, & i > 0 \\ 1, & i \le 0. \end{cases}$$
$$\tag{14}$$

Note that $p\left[\psi(l_{i-1,j})\right]$ is the historical information of the current video frame and it becomes known, when calculating $p\left[\psi(l_{i,j})\right]$, since the coding rates $r_{i-1,1}, \cdots, r_{i-1,n}$ were decided when optimizing the preceding frame $(i - 1)$. Hence, by substituting Eq. (14) into Eq. (11), the expected video distortion $\mathfrak{D}\left(S, l_{i,1}, \cdots, l_{i,n}, r_{i,1}, \cdots, r_{i,n}\right)$ may be further formulated as Eq. (15), as shown at the bottom of this page.

We now derive the transmit SNR s_i of frame f_i in Eq. (3). Based on the conditions in Eq. (4), the transmit power conversion may be expressed as

$$\frac{e_i}{E_b} = \frac{\sum\limits_{j=1}^{n} \left|l_{i,j}\right|}{\sum\limits_{j=1}^{n} \left|x_{i,j}\right|} = r_i. \tag{16}$$

Furthermore, based on the coding rate definition $r_{i,j} = \frac{|l_{i,j}|}{|x_{i,j}|}$, the transmit power conversion of Eq. (16) may be further formulated as

$$e_i = \frac{E_b \cdot \sum\limits_{j=1}^{n} \left|l_{i,j}\right|}{\sum\limits_{j=1}^{n} \frac{|l_{i,j}|}{r_{i,j}}} = E_b \cdot r_i. \tag{17}$$

$$\mathfrak{D}\left(S, l_{i,1}, \cdots, l_{i,n}, r_{i,1}, \cdots, r_{i,n}\right) = \sum_{j=1}^{n} d(l_{i,j}) \cdot \left[1 - \left[1 - \hbar\left(s_i, r_{i,j}\right)\right]^{\frac{|l_{i,j}|}{\lambda}}\right] \cdot p\left[\psi(l_{i-1,j})\right] \cdot \prod_{k=1}^{j-1} \left[1 - \hbar\left(s_i, r_{i,j}\right)\right]^{\frac{|l_{i,k}|}{\lambda}} \tag{15}$$

Based on the definition of the SNR, we have

$$\begin{cases} s_i = 10 \cdot \log_{10} \dfrac{e_i}{N_0} \\ S = 10 \cdot \log_{10} \dfrac{E_b}{N_0}. \end{cases} \tag{18}$$

By substituting the transmit power of Eq. (17) into Eq. (18), the estimated transmit SNR of frame f_i may be expressed as

$$s_i = 10 \cdot \log_{10} \frac{E_b \cdot r_i}{N_0}$$

$$= S - 10 \cdot \log_{10} \frac{\sum\limits_{j=1}^{n} |l_{i,j}|}{N_0 \cdot \sum\limits_{j=1}^{n} \frac{|l_{i,j}|}{r_{i,j}}}. \tag{19}$$

Based on the above derivation, by substituting the transmit SNR of Eq. (19) into the distortion estimation of Eq. (15), our OF of Eq. (3) may be formulated as in Eq. (21), as shown at the bottom of this page, *subject to the condition of*

$$\sum_{j=1}^{n} \frac{|l_{i,j}|}{r_{i,j}} \leq t_i = T \cdot \frac{g}{\mathfrak{F}} \cdot \frac{|f_i|}{\sum\limits_{j=1}^{g} |f_j|}. \tag{20}$$

Note that in Eq. (21), as shown at the bottom of this page, the historical information $p[\psi(l_{i-1,j})]$ was recursively calculated and updated for each frame, which was decided when optimizing frame f_{i-1}. In this paper, we solved the OF in Eqs. (21), (20) using the *fmincon* function of matlab, but a range of other optimization methods may also be employed. Based on the upper-bound bitrate t_i of Eq. (20), the related coding rate optimization procedure of frame f_i is detailed in Algorithm 1, where t_i is pre-calculated using Eq. (20).

D. OVERHEADS

All the optimization operations detailed in Section III are carried out at the transmitter of Fig. 5. Below, we discuss the overheads imposed by this optimization process at the transmitter, noting that some overheads are also imposed at the receiver. Explicitly, the overheads imposed at the transmitter include the estimation of $d(\cdot)$, the generation of the LUT $\hbar(s, r)$, the optimization process and the frame

---

Algorithm 1 Determining the Coding Rates of Frame f_i

1: **inputs:**
    $S, l_{i,1}, \cdots, l_{i,n}, d(l_{i,1}), \cdots, d(l_{i,n}), t_i$
2: **initialize:**
    $p[\psi(l_{0,j})] \leftarrow 1, 1 \leq j \leq n$
        ▷ historical information for first frame
    $dist \leftarrow +\infty$
3: **for each** initial point $\{r_{i,1}, \cdots, r_{i,n}\}$ **do**
4:                           ▷ determining the code rates
5:     $tmp \leftarrow \min \mathfrak{D}(S, l_{i,1}, \cdots, l_{i,n}, r_{i,1}, \cdots, r_{i,n})$
6:     **if** $tmp < dist$ **then**
7:         $dist \leftarrow tmp$
8:         $\hat{r}_{i,1}, \cdots, \hat{r}_{i,n} \leftarrow r_{i,1}, \cdots, r_{i,n}$
9:         $\hat{s}_i \leftarrow s_i$
10:     **end if**
11: **end for**
12: **for** $1 \leq j \leq n$ **do**   ▷ update historical information
13:     $p[\psi(l_{i,j})] \leftarrow p[\psi(l_{i-1,j})] \cdot \prod\limits_{k=1}^{j-1}[1 - \hbar(s_i, r_{i,j})]^{\frac{|l_{i,k}|}{l}}$
14: **end for**
15: **outputs:**
    $\hat{r}_{i,1}, \cdots, \hat{r}_{i,n}$

---

delay imposed. The generation of the LUT $\hbar(s, r)$ only imposes extra off-line processing, while the estimation of $d(\cdot)$ and the optimization process itself impose extra on-line run-time complexity.

1) ESTIMATION OF $d(\cdot)$

As mentioned in Section III-A, $d(l_{i,j})$ is estimated in a similar manner to the procedure of [7], [24], and [39], where the complexity imposed is linearly proportional to n.

2) GENERATION OF THE LUT $\hbar(s, r)$

The LUT $\hbar(s, r)$ is generated by our proposed solution, which is specific for the channel, the STBC decoder and the FEC decoder, as shown in Fig. 7. Hence this table has to be regenerated, when the any of these components is changed. Specifically, the three-dimensional LUT $\hbar(s, r)$

$$\arg \min_{r_{i,1}, \cdots, r_{i,n}} \mathfrak{D}(S, l_{i,1}, \cdots, l_{i,n}, r_{i,1}, \cdots, r_{i,n})$$

$$= \arg \min_{r_{i,1}, \cdots, r_{i,n}} \sum_{j=1}^{n} d(l_{i,j}) \cdot \left[1 - \left[1 - \hbar\left(S - 10 \cdot \log_{10} \frac{\sum\limits_{v=1}^{n} |l_{i,v}|}{N_0 \cdot \sum\limits_{v=1}^{n} \frac{|l_{i,v}|}{r_{i,v}}}, r_{i,j} \right) \right]^{\frac{|l_{i,j}|}{\lambda}} \right]$$

$$\cdot p[\psi(l_{i-1,j})] \cdot \prod_{k=1}^{j-1} \left[1 - \hbar\left(S - 10 \cdot \log_{10} \frac{\sum\limits_{v=1}^{n} |l_{i,v}|}{N_0 \cdot \sum\limits_{v=1}^{n} \frac{|l_{i,v}|}{r_{i,v}}}, r_{i,k} \right) \right]^{\frac{|l_{i,k}|}{\lambda}} \tag{21}$$

TABLE 4. Parameters for transmitting the employed RaceHorses sequence.

Parameters	RaceHorses
Representation	YUV 4:2:0
Format	416×240
Bits Per Pixel	8
FPS	30
No. of Frames	30
No. of Layers/Frame	3
Video Codec	SHVC
GOP	4
Bitrate (Mbps)	3.9
QPs/Frame	40, 30, 20
Error-Free Y-PSNR (dB)	27.7, 33.4, 41.4
Error Concealment	Frame-Copy
FEC	RSC [11,11,13,17]
QAM	4QAM (2bits/symbol)
STBC	2×2
No. of FSO Apertures	2
Optical Wavelength	1.55 μm
Simulations Repeated	100

is generated by simulations by sweeping through the variables s and r. *Moreover, the LUT is independent of the specific video sequences and it is generated during the design process.* By assuming that n_s and n_r indicate the number of variables s and r, the size of LUT may be calculated as $(n_s \times n_r)$.

3) OPTIMIZATION PROCESS
Again, the optimization process is carried out by the *fmincon* function of matlab. Specifically, the adaptive particle swarm optimization (APSO) technique of [43] may be readily employed for finding the global optimum in real-time. Note that in the scenarios, where as few as 2-4 layers are considered, even a full search may be realistic.

4) DELAY
As discussed in Section III, the coding rates of g frames are considered as an optimization group limited by the bitrate upper bound of $\frac{g}{f} \cdot T$. Hence a maximum delay of g video frames is imposed. Note that the parameter g may be adjusted depending on the specific applications having different delay requirements.

IV. SYSTEM PERFORMANCE
In this section, we benchmark our proposed HA-UEP-FSO system against the traditional equal error protection (EEP) aided SHVC-FSO system (EEP-FSO). The parameters of the video sequences employed in the simulations are listed in Table 4. The 4:2:0 YUV format (416×240)-pixel resolution based RaceHorses video clip was encoded by the

SHVC reference software SHM, where the "frame-copy" based error concealment was activated for replacing the corrupted frames. The GOP duration was set to 4, while the RACs of IDR/CDR frames were inserted every 4 frames. The B frames were disabled in our SHVC configuration for the sake of limiting the delay and hence supporting flawless lip-synchronization. Correspondingly, the video sequence was encoded into GOPs, consisting of an I frame, followed by P frames. Additionally, only the quality-scalability feature [10], [44] was enabled, when encoding the video sequences into three different-quality layers, namely into the layers $l_{i,1}$, $l_{i,2}$ and $l_{i,3}$ using the standard H.265 quantization parameters (QPs) of 40, 30 and 20, respectively. Furthermore, each video frame was encoded into a single BL and two ELs, resulting in three network abstraction layer units (NALUs). These configurations jointly resulted in a bitrate of 3.9 Megabits per second (Mbps) at 30 FPS. Furthermore, in the absence of transmission errors, the Y-PSNR (dB) of 27.7, 33.4, 41.4 may be achieved by reconstructing the video from the layer sets of $\{l_{i,1}\}$, $\{l_{i,1}, l_{i,2}\}$ and $\{l_{i,1}, l_{i,2}, l_{i,3}\}$, respectively. All the parameters employed are detailed in Table 4.

Apart from the source configurations detailed above, the FEC and the transmission parameters are configured as follows. An RSC codec configured by the generator polynomials of [1011, 1011, 1101, 1111] was employed as the FEC codec. Moreover, 4QAM and the 2×2 structured STBC are employed for generating the encoded signals, which were then transmitted through 2 FSO apertures. Each SHVC-compressed bitstream was channel encoded and transmitted on a NALU by NALU [9] basis, which is the smallest unit to be decoded by the SHVC decoder. Each NALU was protected by cyclic redundancy check (CRC) codes. At the receiver, each decoded NALU failing to pass the CRC check process was removed before the SHVC video decoding process. In all of our experiments, the simulations were repeated 100 times in order to generate statistically sound performance curves. All the parameters employed are detailed in Table 4.

A. OFF-LINE LUT GENERATION
In our experiments, the vectors of $[-5 : 0.5 : 25]$, $[0 : 0.1 : 4]^4$ are utilized for the variables s, r^{-1} of $\hbar(s, r)$, respectively, for generating the LUT, which result in $n_s = 61$, $n_r = 41$. Moreover, the packet length of $\lambda = 1000$ is employed and 8-byte floating values were utilized for storing the LUT in memory.

B. PERFORMANCE FOR g = 4
Below, we evaluate the PSNR video quality, the PER and the BER of layers, as well as the bitrate of the scenarios associated with the upper-bound bitrates of $T = 3.9$ Mbps, $T = 11.6$ Mbps and $T = 19.4$ Mbps. Moreover, a frame delay of $g = 4$ is employed, while the video quality versus delay will be presented in Section IV-C.

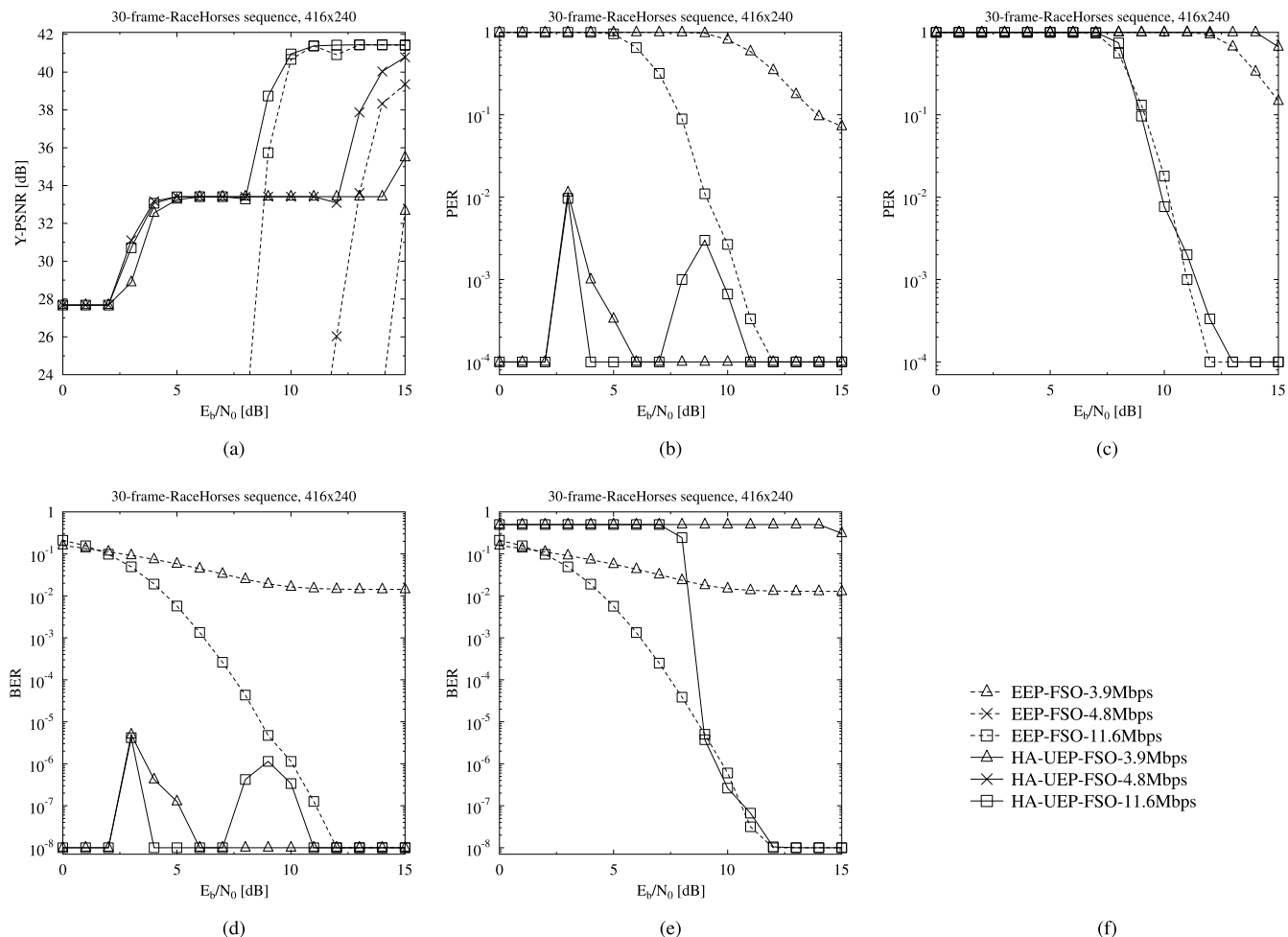[4]These values can be stored as floats in 8 bytes each.

FIGURE 9. PSNR, PER, BER versus E_b/N_0 performance comparison of the proposed system and the benchmarkers, namely the HA-UEP-FSO scheme, the EEP-FSO scheme for the *RaceHorses* sequence with system throughput T = 3.9, 4.8, 11.6 Mbps. (a) PSNR vs E_b/N_0. (b) PER vs E_b/N_0, $l_{\cdot,1}$. (c) PER vs E_b/N_0, $l_{\cdot,3}$. (d) BER vs E_b/N_0, $l_{\cdot,1}$. (e) BER vs E_b/N_0, $l_{\cdot,3}$. (f) Tested schemes.

1) VIDEO QUALITY

The PSNR video quality versus system throughput and channel E_b/N_0 is portrayed in Fig. 10. Specifically, we observe that the performance of both HA-UEP-FSO and EEP-FSO improves upon increasing the system through-put or the channel's E_b/N_0. Moreover, the HA-UEP-FSO surface indicates a better performance than the EEP-FSO surface, especially in the lower range of the system's throughput or of the channel E_b/N_0.

The PSNR versus E_b/N_0 results were recorded in Fig. 9a, where the HA-UEP-FSO scheme is seen to substantially out-perform the EEP-FSO scheme, especially in the lower E_b/N_0 range. This is because the EEP-FSO scheme does not have the capability of gracefully reducing the video-rate by refraining from transmitting all enhancement layers, when the chan-nel SNR or channel throughput is decreasing. By contrast, the HA-UEP-FSO scheme is capable of dropping or adding enhancement layers, as well as selecting the suitable coding rates for the different layers, which results in the staircase-shaped curves in Fig. 9a.

Specifically, in the E_b/N_0 range of 0 dB to 2 dB, the HA-UEP-FSO scheme achieves a PSNR of 27.7 dB for sys-tem throughput of 3.9, 4.8, 11.6 Mbps, where only the first layer is received correctly. Moreover, a PSNR of 33.4 dB is achieved in the E_b/N_0 range of 4 dB to 8 dB, where two layers may be correctly received. By comparison, the EEP-FSO scheme is unable to reconstruct the video at E_b/N_0 val-ues below 8 dB for the T = 11.6 Mbps scenario. At T = 11.6 Mbps, the HA-UEP-FSO scheme outper-forms the EEP-FSO scheme by about 4.5 dB E_b/N_0 at a PSNR of 33 dB.

Furthermore, the benchmarkers associated with the 11.6 Mbps bitrate substantially outperform the 3.9 Mbps scenario for both the HA-UEP-FSO and EEP-FSO scheme. This is due to the fact that for the 11.6 Mbps scenario, lower FEC coding rates are allocated than for 3.9 Mbps.

2) PER AND BER OF LAYERS

The PER versus E_b/N_0 results recorded for layers $l_{\cdot,1}$ and $l_{\cdot,3}$ are displayed in Fig. 9b and Fig. 9c, respectively. In Fig. 9b, we observe again that the HA-UEP-FSO substantially
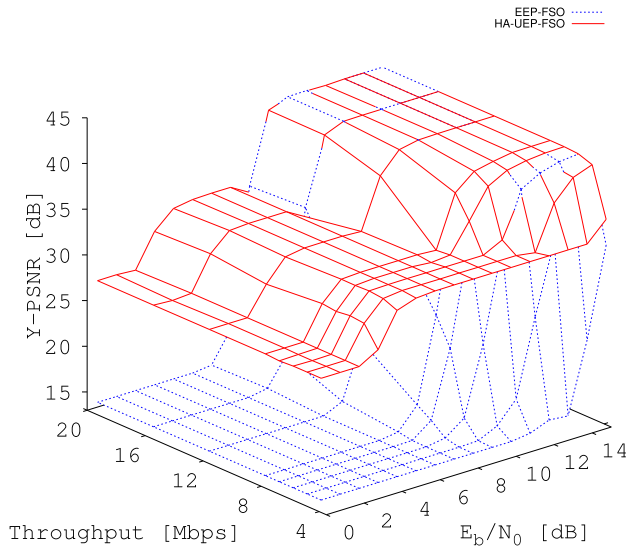
FIGURE 10. PSNR video quality versus system throughput and channel E_b/N_0 comparison of the proposed system and of the benchmarks, namely of the HA-UEP-FSO scheme, and of the EEP-FSO scheme for the *RaceHorses* video sequence.
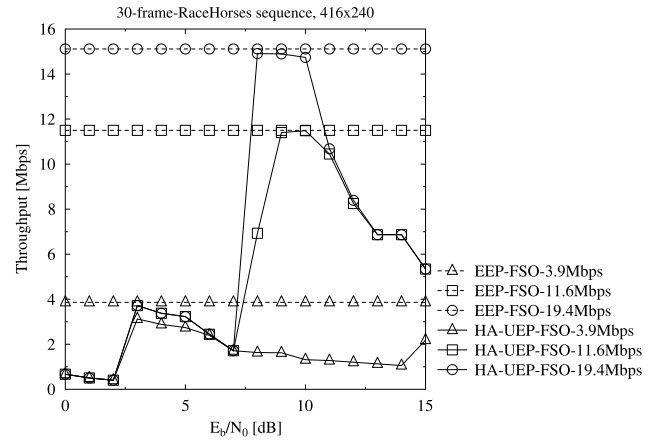

FIGURE 11. Required throughput versus E_b/N_0 performance comparison of the proposed system and of the benchmarks, namely of the HA-UEP-FSO scheme, and of the EEP-FSO scheme for the *RaceHorses* video sequence.
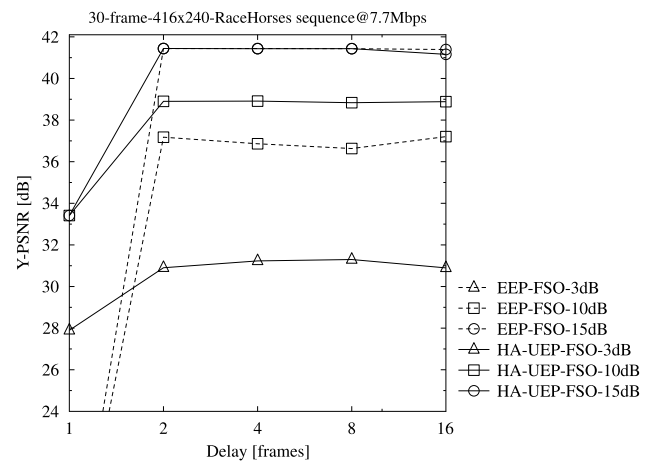

FIGURE 12. PSNR versus frame delay comparison of the proposed system and of the benchmarks at $T = 7.7$ Mbps, namely of the HA-UEP-FSO scheme, and of the EEP-FSO scheme for the *RaceHorses* sequence.

outperforms the EEP-FSO scheme. The HA-UEP-FSO scheme associated with a bitrate of $T = 11.6$ Mbps has two PER peaks, namely at $E_b/N_0 = 3$ dB, and 9 dB.[5] This is due to the fact that the protection of the BL is reduced for the sake of better protecting the ELs, when we have an increasing E_b/N_0. This may also be illustrated by comparing Fig. 9a and Fig. 9b, where substantial PSNR and PER improvements are observed both at E_b/N_0 values of 3 dB and 9 dB. Similar trends are also observed for the HA-UEP-FSO scheme associated with $T = 3.9$ Mbps. In Fig. 9c, as expected the HA-UEP-FSO outperforms the EEP-FSO scheme having $T = 3.9$ Mbps. This is due to the fact that the protection of layer $l_{,2}$ is sacrificed for the sake of better protecting layer $l_{,1}$ in the HA-UEP-FSO scheme.

The BER versus E_b/N_0 trends observed in Fig. 9d and Fig. 9e are similar to those of Fig. 9b and Fig. 9c.

3) BITRATE

In Fig. 11, the trends seen in Fig. 9b become more explicit. To elaborate, the EE-FSO schemes maintain a constant bitrate regardless of the channel SNR, hence their PSNR becomes unacceptable at low SNRs in Fig. 9a. By contrast, our HA-UEP-FSO scheme is capable of adapting the number of ELs, hence accommodating the SNR fluctuations without excessive PERs. Therefore, it maintains a slightly reduced-resolution video-quality, which is however free from variable transmission powers.

C. VIDEO QUALITY VERSUS DELAY

Fig. 12 shows the PSNR versus frame delay trends of the benchmarks and of the proposed solution at E_b/N_0 of 3 dB, 10 dB, 15 dB evaluated for $T = 7.7$ Mbps. We observe

[5]In the simulations, the PER values of 0 are replaced by 10^{-4} for the sake of visibly showing the trends of the curves.

substantial PSNR improvements upon increasing the delay from $g = 1$ to $g = 2$ for all the curves, but the PSNR no longer improves over the range of $g = 2$ to $g = 16$. This may be attributed to the fact that we insert a CDR every 4 frames. Moreover, HA-UEP-FSO substantially outperforms the EEP-FSO scheme for all SNR values.

V. CONCLUSIONS

We proposed the HA-UEP concept for video communications over FSO channels. Our OF was designed by carefully exploiting the layer dependencies both of the current frame and of the historical frames. By solving the OF, a specific subset of the layers may be selected in conjunction with the appropriately determined FEC coding rates, where the video distortion is minimized under the constraint of a specific throughput. Our simulation results show that the proposed system outperforms the traditional EEP scheme by about 4.5 dB of E_b/N_0 at a PSNR of 33 dB.

In our future work, we may incorporate our previous inter-layer FEC technique of [22] and [24] into our

HA-UEP-FSO system. Furthermore, we may also consider to unequally allocate the bitrate to different video frames within a GOP.
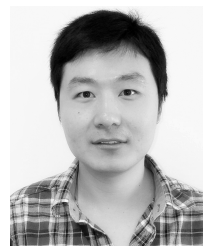
GLOSSARY

3D	Three-Dimensional.
ACO	Asymmetrically Clipped Optical.
APSO	Additive Particle Swarm Optimization.
AVC	Advanced Video Coding.
BL	Base Layer.
BPS	Bits Per Second.
CC	Convolutional Codes.
CDR	Clean Decoder Refresh.
CIF	Common Intermediate Format.
CRC	Cyclic Redundancy Check.
DVC	Distributed Video Coding.
EEP	Equal Error Protection.
EL	Enhancement Layer.
FEC	Forward Error Correction.
FSO	Free Space Optical.
GOP	Group Of Pictures.
HA	Historical information Aware.
HD	High Definition.
HEVC	High-Efficiency Video Coding.
IDR	Instantaneous Decoding Refresh.
IL-FEC	Inter-Layer Forward Error Correction.
IR	Infrared.
LDPC	Low-Density Parity-Check.
LUT	LookUp Table.
Mbps	MegaBits Per Second.
MIMO	Multiple Input Multiple Output.
ML	Maximum-Likelihood.
MPEG	Moving Picture Experts Group.
MVP	MultiView Profile.
NALU	Network Abstraction Layer Unit.
OF	Objective Function.
OFDM	Orthogonal Frequency-Division Multiplexing.
OWC	Optical Wireless Communication.
PER	Packet Error Ratio.
PSNR	Peak Signal-to-Noise Ratio.
QAM	Quadrature Amplitude Modulation.
QCIF	Quarter Common Intermediate Format.
QP	Quantization Parameter.
RAC	Random Access Points.
RCPC	Rate-Compatible Convolutional Code.
RSC	Recursive Systematic Convolutional.
SHM	SHVC Reference Software.
SHVC	Scalable High Efficiency Video Coding.
SI	Side Information.
SNR	Signal-to-Noise Ratio.
STBC	Space-Time Block Code.
SVC	Scalable Video Coding.
UEP	Unequal Error Protection.
WZ	Wyner-Ziv.

REFERENCES

[1] L. Hanzo, P. J. Cherriman, and J. Streit, *Video Compression and Communications: From Basics to H.261, H.263, H.264, MPEG4 for DVB and HSDPA-Style Adaptive Turbo-Transceivers.* New York, NY, USA: Wiley, 2007.

[2] Y. Huo, M. El-Hajjar, and L. Hanzo, "Wireless video: An interlayer error-protection-aided multilayer approach," *IEEE Veh. Technol. Mag.*, vol. 9, no. 3, pp. 104–112, Sep. 2014.

[3] H. Imaizumi and A. Luthra, "MPEG-2 multiview profile," in *Three-Dimensional Television, Video, and Display Technologies.* Berlin, Germany: Springer-Verlag, 2002, pp. 169–181.

[4] H. Schwarz, D. Marpe, and T. Wiegand, "Overview of the scalable video coding extension of the H.264/AVC standard," *IEEE Trans. Circuits Syst. Video Technol.*, vol. 17, no. 9, pp. 1103–1120, Sep. 2007.

[5] *AVC: Advanced Video Coding for Generic Audio Visual Services*, Standard ITUT Rec. H.264 and ISO/IEC 1449610 (AVC), ITUT and ISO/IEC JTC 1, Mar. 2010

[6] A. Vetro, T. Wiegand, and G. J. Sullivan, "Overview of the stereo and multiview video coding extensions of the H.264/MPEG-4 AVC standard," *Proc. IEEE*, vol. 99, no. 4, pp. 626–642, Apr. 2011.

[7] Y. Huo, C. Hellge, T. Wiegand, and L. Hanzo, "A tutorial and review on inter-layer FEC coded layered video streaming," *IEEE Commun. Surveys Tuts.*, vol. 17, no. 2, pp. 1166–1207, 2nd Quart., 2015.

[8] G. J. Sullivan, J.-R. Ohm, W.-J. Han, and T. Wiegand, "Overview of the high efficiency video coding (HEVC) standard," *IEEE Trans. Circuits Syst. Video Technol.*, vol. 22, no. 12, pp. 1649–1668, Dec. 2012.

[9] *High Efficiency Video Coding*, Standard ITUT, H.265, ISO/IEC MPEG and ITUT VCEG, Apr. 2015.

[10] P. Helle *et al.*, "A scalable video coding extension of HEVC," in *Proc. IEEE Data Compress. Conf. (DCC)*, Mar. 2013, pp. 201–210.

[11] B. Masnick and J. Wolf, "On linear unequal error protection codes," *IEEE Trans. Inf. Theory*, vol. 13, no. 4, pp. 600–607, Oct. 1967.

[12] F. Marx and J. Farah, "A novel approach to achieve unequal error protection for video transmission over 3G wireless networks," *Signal Process., Image Commun.*, vol. 19, no. 4, pp. 313–323, 2004.

[13] V. Pavlushkov, R. Johannesson, and V. V. Zyablov, "Unequal error protection for convolutional codes," *IEEE Trans. Inf. Theory*, vol. 52, no. 2, pp. 700–708, Feb. 2006.

[14] J. Hagenauer, "Rate-compatible punctured convolutional codes (RCPC codes) and their applications," *IEEE Trans. Commun.*, vol. 36, no. 4, pp. 389–400, Apr. 1988.

[15] V. Kumar and O. Milenkovic, "On unequal error protection LDPC codes based on plotkin-type constructions," *IEEE Trans. Commun.*, vol. 54, no. 6, pp. 994–1005, Jun. 2006.

[16] R. G. Gallager, *Low-Density Parity-Check Codes*. Cambridge, MA, USA: MIT Press, 1963.

[17] N. Rahnavard, H. Pishro-Nik, and F. Fekri, "Unequal error protection using partially regular LDPC codes," *IEEE Trans. Commun.*, vol. 55, no. 3, pp. 387–391, Mar. 2007.

[18] M. Aydinlik and M. Salehi, "Turbo coded modulation for unequal error protection," *IEEE Trans. Commun.*, vol. 56, no. 4, pp. 555–564, Apr. 2008.

[19] Y. C. Chang, S. W. Lee, and R. Komyia, "A fast forward error correction allocation algorithm for unequal error protection of video transmission over wireless channels," *IEEE Trans. Consum. Electron.*, vol. 54, no. 3, pp. 1066–1073, Aug. 2008.

[20] Y. C. Chang, S. W. Lee, and R. Komiya, "A low complexity hierarchical QAM symbol bits allocation algorithm for unequal error protection of wireless video transmission," *IEEE Trans. Consum. Electron.*, vol. 55, no. 3, pp. 1089–1097, Aug. 2009.

[21] N. Nasruminallah and L. Hanzo, "Near-capacity H.264 multimedia communications using iterative joint source-channel decoding," *IEEE Commun. Surveys Tuts.*, vol. 14, no. 2, pp. 538–564, 2nd Quart., 2012.

[22] Y. Huo, M. El-Hajjar, and L. Hanzo, "Inter-layer FEC aided unequal error protection for multilayer video transmission in mobile TV," *IEEE Trans. Circuits Syst. Video Technol.*, vol. 23, no. 9, pp. 1622–1634, Sep. 2013.

[23] J. J. Micallef, R. A. Farrugia, and C. J. Debono, "Correlation noise-based unequal error protected rate-adaptive codes for distributed video coding," *IEEE Trans. Circuits Syst. Video Technol.*, vol. 24, no. 1, pp. 127–140, Jan. 2013.

[24] Y. Huo, M. El-Hajjar, R. G. Maunder, and L. Hanzo, "Layered wireless video relying on minimum-distortion inter-layer FEC coding," *IEEE Trans. Multimedia*, vol. 16, no. 3, pp. 697–710, Apr. 2014.

[25] A. Vosoughi, P. C. Cosman, and L. B. Milstein, "Joint source-channel coding and unequal error protection for video plus depth," *IEEE Signal Process. Lett.*, vol. 22, no. 1, pp. 31–34, Jan. 2015.

[26] D. Song and C. W. Chen, "Scalable H.264/AVC video transmission over MIMO wireless systems with adaptive channel selection based on partial channel information," *IEEE Trans. Circuits Syst. Video Technol.*, vol. 17, no. 9, pp. 1218–1226, Sep. 2007.

[27] C. Hellge, D. Gomez-Barquero, T. Schierl, and T. Wiegand, "Layer-aware forward error correction for mobile broadcast of layered media," *IEEE Trans. Multimedia*, vol. 13, no. 3, pp. 551–562, Jun. 2011.

[28] S. Cicalo and V. Tralli, "Distortion-fair cross-layer resource allocation for scalable video transmission in OFDMA wireless networks," *IEEE Trans. Multimedia*, vol. 16, no. 3, pp. 848–863, Apr. 2014.

[29] S. X. Ng, J. Y. Chung, P. Cherriman, and L. Hanzo, "Burst-by-burst adaptive decision feedback equalized TCM, TTCM, and BICM for H.263-assisted wireless video telephony," *IEEE Trans. Circuits Syst. Video Technol.*, vol. 16, no. 3, pp. 363–374, Mar. 2006.

[30] L. Hanzo, R. Maunder, T. Wang, and Y. Huo, "Motion-aware mesh-structured trellis for correlation modelling aided distributed multi-view video coding," *IEEE Trans. Image Process.*, vol. 23, no. 1, pp. 319–331, Jan. 2014.

[31] Y. Huo, T. Wang, R. Maunder, and L. Hanzo, "Two-dimensional iterative source-channel decoding for distributed video coding," *IEEE Commun. Lett.*, vol. 18, no. 1, pp. 90–93, Jan. 2014.

[32] M. A. Khalighi and M. Uysal, "Survey on free space optical communication: A communication theory perspective," *IEEE Commun. Surveys Tuts.*, vol. 16, no. 4, pp. 2231–2258, 4th Quart., 2014.

[33] E. Ciaramella *et al.*, "1.28-Tb/s (32×40 Gb/s) free-space optical WDM transmission system," *IEEE Photon. Technol. Lett.*, vol. 21, no. 16, pp. 1121–1123, Aug. 15, 2009.

[34] N. Cvijetic, S. G. Wilson, and R. Zarubica, "Performance evaluation of a novel converged architecture for digital-video transmission over optical wireless channels," *J. Lightw. Technol.*, vol. 25, no. 11, pp. 3366–3373, Nov. 2007.

[35] R. Llorente and M. Morant, "Audio and video service provision in deep-access integrated optical-wireless networks," in *Proc. 22nd Eur. Signal Process. Conf. (EUSIPCO)*, Sep. 2014, pp. 1895–1899.

[36] J. Armstrong and A. J. Lowery, "Power efficient optical OFDM," *Electron. Lett.*, vol. 42, no. 6, pp. 370–372, Mar. 2006.

[37] J. Jiang, P. Zhang, R. Zhang, S. Chen, and L. Hanzo, "Aperture selection for ACO-OFDM in free-space optical turbulence channel," *IEEE Trans. Veh. Technol.*, vol. 65, no. 8, pp. 6089–6100, Aug. 2016.

[38] M. A. Al-Habash, L. C. Andrews, and R. L. Phillips, "Mathematical model for the irradiance probability density function of a laser beam propagating through turbulent media," *Opt. Eng.*, vol. 40, no. 8, pp. 1554–1562, Aug. 2001.

[39] H. Ha and C. Yim, "Layer-weighted unequal error protection for scalable video coding extension of H.264/AVC," *IEEE Trans. Consum. Electron.*, vol. 54, no. 2, pp. 736–744, May 2008.

[40] X. K. Yang *et al.*, "Unequal loss protection for robust transmission of motion compensated video over the Internet," *Signal Process., Image Commun.*, vol. 18, no. 3, pp. 157–167, 2003.

[41] E. Maani and A. Katsaggelos, "Unequal error protection for robust streaming of scalable video over packet lossy networks," *IEEE Trans. Circuits Syst. Video Technol.*, vol. 20, no. 3, pp. 407–416, Mar. 2010.

[42] R. Khalili and K. Salamatian, "A new analytic approach to evaluation of packet error rate in wireless networks," in *Proc. 3rd Annu. Commun. Netw. Services Res. Conf.*, Halifax, NS, Canada, May 2005, pp. 333–338.

[43] Z.-H. Zhan, J. Zhang, Y. Li, and S.-H. Chung, "Adaptive particle swarm optimization," *IEEE Trans. Syst., Man, Cybern. B, Cybern.*, vol. 39, no. 6, pp. 1362–1381, Dec. 2009.

[44] G. J. Sullivan, J. M. Boyce, Y. Chen, J.-R. Ohm, C. A. Segall, and A. Vetro, "Standardized extensions of high efficiency video coding (HEVC)," *IEEE J. Sel. Topics Signal Process.*, vol. 7, no. 6, pp. 1001–1016, Dec. 2013.
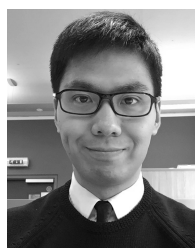
Cheng Zhou received the B.S. degree in electronics and information engineering from Hubei University, Wuhan, China, in 2001, and the M.S. degree in pattern recognition and intelligent systems and the Ph.D. degree in control science and engineering from the Huazhong University of Science and Technology, Wuhan, in 2007 and 2010, respectively. He was a Visiting Scholar with the School of Electronics and Computer Science, University of Southampton from 2013 to 2014. He is currently a Lecturer with the School of Electronics and Information Engineering, South-Central University for Nationalities, Wuhan. His research interests include multimedia signal processing, particularly, video coding for MPEG-4, H.264, AVS (China), and HEVC standards, since 2004.

Junyi Jiang received the B.Eng. degree in communication engineering from the Heilongjiang Institute of Science and Technology, China, in 2009, the M.Sc. degree (Hons.) in wireless communication from the University of Southampton, U.K., in 2010, and the Ph.D. degree from the Southampton Wireless Group, University of Southampton. His research interests include indoor visible light communication, free-space optical communication, and iterative detection. He is currently with the Huawei Technologies.

Yongkai Huo received the B.Eng. degree (Hons.) in computer science and technology from the Hefei University of Technology, Hefei, China, in 2006, the M.Eng. degree in computer software and theory from the University of Science and Technology of China, Hefei, in 2009, and the Ph.D. degree with the Wireless Communications Group, School of Electronics and Computer Science, University of Southampton, Southampton, U.K., in 2014, where he is currently a Research Fellow. He has authored a number of research papers in distributed video coding, multiview video coding, robust wireless video streaming, and joint source-channel decoding. He received a scholarship under the China–U.K. Scholarships for Excellence Programme.

Lajos Hanzo (F'04) received the D.Sc. degree in electronics in 1976 and the Ph.D. degree in 1983. Since 1986, he has been with the School of Electronics and Computer Science, University of Southampton, U.K., where he holds the Chair in telecommunications. He has successfully supervised over 100 Ph.D. students, co-authored 20 John Wiley/IEEE Press books on mobile radio communications totaling in excess of 10, 000 pages, and authored 1581 research entries at the IEEE Xplore. He is a fellow of FREng, FIET, and EURASIP. He was acted as a TPC and the General Chair of the IEEE conferences, presented keynote lectures, and has been awarded a number of distinctions. In 2009, he received the honorary doctorate Doctor Honoris Causa by the Technical University of Budapest. During his 38-year career in telecommunications, he has held various research and academic posts in Hungary, Germany, and U.K. He is currently directing a 60 strong Academic Research Team, working on a range of research projects in wireless multimedia communications sponsored by industry, the Engineering and Physical Sciences Research Council, U.K., the European Research Council's Advanced Fellow Grant, and the Royal Society's Wolfson Research Merit Award. He is an Enthusiastic Supporter of industrial and an Academic Liaison, and he offers a range of industrial courses. He is also the Governor of the IEEE VTS. From 2008 to 2012, he was the Editor-in-Chief of the IEEE Press and a Chaired Professor also at Tsinghua University, Beijing. His research is funded by the European Research Council's Senior Research Fellow Grant. He has over 25, 000 citations.

● ● ●